processes

MDPI

Article

New Evidence of the Effect of Post-Combustion During Roasting/Reduction of Nickel-Bearing Lateritic Ores

Hugo Javier Angulo Palma [1,2,*], Norman Toro [3], Jonathan Castillo [4], Felipe M. Galleguillos Madrid [5], Iván Salazar [6], Ingrid Jamett [7,8], Eleazar Salinas-Rodríguez [9] and Manuel Saldana [3,10,*]

1 Centro de Investigaciones del Níquel "Capitán Alberto Fernández Montes de Oca" (CEDINIQ), Moa 83330, Holguín, Cuba
2 Facultad de Metalurgia y Electromecánica, Universidad de Moa (UMoa), Moa 83330, Holguín, Cuba
3 Faculty of Engineering and Architecture, Universidad Arturo Prat, Iquique 1110939, Chile; notoro@unap.cl
4 Departamento de Ingeniería en Metalurgia, Universidad de Atacama, Copiapó 1530000, Chile; jonathan.castillo@uda.cl
5 Centro de Desarrollo Energético Antofagasta, Universidad de Antofagasta, Antofagasta 1270300, Chile; felipe.galleguillos.madrid@uantof.cl
6 Departamento de Ingeniería Civil, Universidad Católica del Norte, Antofagasta 1270709, Chile; isalazar@ucn.cl
7 Departamento de Ingeniería Industrial, Facultad de Ingeniería, Universidad de Antofagasta, Antofagasta 1270300, Chile; ingrid.jamett@uantof.cl
8 Centro de Economía Circular en Procesos Industriales (CECPI), Facultad de Ingeniería, Universidad de Antofagasta, Antofagasta 1270300, Chile
9 Academic Area of Earth Sciences and Materials, Institute of Basic Sciences and Engineering, Autonomous University of the State of Hidalgo, Pachuca 42184, Mexico; salinasr@uaeh.edu.mx
10 Departamento de Ingeniería Química y Procesos de Minerales, Universidad de Antofagasta, Antofagasta 1270300, Chile
* Correspondence: hangulo@cil.moa.minem.cu (H.J.A.P.); masaldana@unap.cl (M.S.); Tel.: +56-953834174 (M.S.)

Abstract

The roasting/reduction process is one of the fundamental stages of Caron technology, ensuring the adequate transformation of lateritic ore, with post-combustion air feed being one of the main variables considered. In this study, new evidence is presented that justifies the negative effect that post-combustion air has on Ni extractions in H-6 of the furnace. With this objective, three air feed levels were evaluated, measuring the hearth temperature from 495 °C without post-combustion to 780 °C for the maximum post-combustion level analyzed. The evaluation was carried out in a conventional multi-hearth furnace at pilot scale using atomic absorption spectrometry, XRD, SEM, and particle size analysis as the main analytical techniques for the characterization of lateritic ore before and after the reduction process. Increasing the temperature of H-6 resulted in a significant decrease in Ni extractions by 1.68% for every 57 °C increase in hearth temperature, which was due to the resulting decrease in the reaction rate constant and the significant increase in the average particle size of the reduced ore. This research emphasizes the importance of controlling post-combustion air inflow as a technological alternative to optimize Ni extraction and reduce delays in the control of diffusive processes.

Keywords: nickel extraction; post-combustion; roasting/reduction in the Caron process; lateritic minerals; thermochemical processing

check for updates

Academic Editor: Haibin Zuo

Received: 23 May 2025
Revised: 6 July 2025
Accepted: 12 August 2025
Published: 17 August 2025

Citation: Palma, H.J.A.; Toro, N.; Castillo, J.; Galleguillos Madrid, F.M.; Salazar, I.; Jamett, I.; Salinas-Rodríguez, E.; Saldana, M. New Evidence of the Effect of Post-Combustion During Roasting/Reduction of Nickel-Bearing Lateritic Ores. *Processes* **2025**, *13*, 2602. https://doi.org/10.3390/pr13082602

Copyright: © 2025 by the authors. Licensee MDPI, Basel, Switzerland. This article is an open access article distributed under the terms and conditions of the Creative Commons Attribution (CC BY) license (https://creativecommons.org/licenses/by/4.0/).

1. Introduction

Nickel (Ni) is a critical and strategic transition metal with high demand in the international market due to its essential use in the production of special and stainless alloys and

its excellent electrical conductivity and chemical stability [1,2]. Recently, as a consequence of the gradual depletion of high-Ni-sulfide ores, its extraction from lateritic ore processing has received significant attention [3–6].

Currently, one of the main technologies that exist for the extraction of Ni from lateritic ores is the Caron process, with more than 100 years of experience from the time it was patented [7,8]. It is a technology that selectively extracts Ni by combining pyro-hydrometallurgical processes, obtaining the maximum levels of efficiency when feeding lateritic ores, with a predominance of the mineralogical phases of iron oxides and oxy-hydroxides (Fe) with mass percentages of Ni and Fe greater than 0.9% and 25%, respectively [9,10].

In general, the Caron process is carried out using the fundamental operations of drying, grinding, roasting/reduction, and leaching [11,12]—the roasting/reduction stage being one of the most important [13–15]. The roasting/reduction stage is key to ensuring an adequate transformation of the lateritic ore fed to the process, guaranteeing the maximum possible conversion of NiO into metallic nickel (Nio) when reacting with CO, which is formed from the fuels used [16–18]. Different investigations recognize that the characteristics of the lateritic ore [19–21], the operations of the multiple-hearth furnace [10,12,14,15,22–24], and the use of reducing additives [9,13,25–28] constitute the most important variables to control during the roasting/selective reduction process.

When considering the variables that influence the operations of multiple-hearth furnaces at commercial scales, one of the most controversial in the scientific community is the feeding of post-combustion air [10]. Post-combustion is the process that occurs as a consequence of the injection of secondary air into hearths four and six to burn excess reducing gases, achieve energy recovery, and preserve the integrity of the furnace [29]. The use of post-combustion in multiple-hearth furnaces generates considerable changes in the concentration of the reducing atmosphere in the upper hearths; its control is a very important operation [30,31]. More recently, some research [10,23] considers the negative effect of post-combustion on nickel extraction when lateritic ores with a predominance of Fe oxide and oxy-hydroxide phases are fed to the furnace; however, to date, no evidence has been presented to justify this behavior.

Thus, the objective of this study is to justify the negative effect of the use of post-combustion during the roasting/reduction stage of the Caron process. For this aim, this study includes a kinetic analysis of the pilot-scale roasting/reduction process with various levels of post-combustion air feed, as well as an X-ray diffraction analysis of the lateritic ore fed to the furnace, scanning electron microscopy, and particle size analysis of the reduced ore. Finally, the results obtained demonstrate that the negative effect of post-combustion is due to the changes it generates in the reaction rate constant of the roasting/reduction process, as well as its influence on the size and shape of the reduced ore particles.

2. Materials and Methods

2.1. Chemical-Physical Characteristics of the Lateritic Ore

In this study, a mixture of nickel-bearing lateritic ores, predominantly Fe oxides and oxyhydroxides, from Moa deposits in Cuba, was used. The chemical and physical characteristics of the mineral and its main mineralogical phases are presented in Table 1 and Figure 1, respectively.

Table 1. Characteristics of the lateritic ore fed to the reduction process.

Content, wt %									Particle Size, µm			
									150	75	45	<45
Ni	Co	Fe	MgO	SiO_2	Al_2O_3	H_2O	S	C	Contribution, %			
1.167	0.099	39.323	2.828	7.788	8.080	3.660	0.251	2.088	3.425	9.783	7.392	79.400

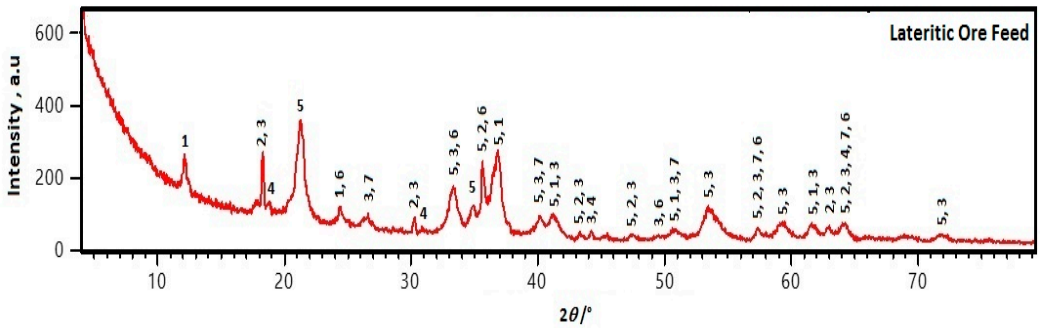

Figure 1. X-ray diffraction pattern of lateritic ore fed to the roasting/reduction process. 1—Lizardite: $Mg_3Si_2O_5(OH)_4$; 2—Maghemite: $Fe_{21.16}O_{31.92}$; 3—Gibbsite: $Al(OH)_3$; 4—Spinel: $MgAl_2O_4$; 5—Goethite: FeOOH; 6—Hematite: Fe_2O_3; 7—Quartz: SiO_2.

2.2. Characteristics of the Experimental Facility

The experiments were carried out in the conventional multiple hearth furnace (see Figure 2) in the pilot plant of the CEDINIQ. The reducing atmosphere was generated from the combustion of fuel oil in the combustion chambers, enriched with the use of the mixture of bituminous coal at 2.0 wt. % and fuel oil at 1.25 wt. % (BC2-FO1.25) as a reducing additive, with characteristics similar to those reported by Angulo et al. [9,32].

In this study, three levels of post-combustion air feed were evaluated in furnace six (H-6) for five days of operation each; their control was ensured by measuring the average temperature of H-6 at 495 °C with no post-combustion, 660 °C with low post-combustion, and 780 °C with high post-combustion. Figure 3 shows the temperature profile used in each furnace zone for each of the experiments ± 5 °C. Additionally, Ni extraction contents were determined using Equation (1), with an uncertainty of ±1.5%, to identify whether significant changes occurred during the evaluation of the different temperature levels in H-6.

$$C_{Ext\text{-}Ni} = \left[1 - \frac{C_{Ni\text{-}leached\ ore} C_{Fe\text{-}fed}}{C_{Ni\text{-}fed} C_{Fe\text{-}leached\ ore}}\right] 100 \quad (1)$$

where

$C_{Ext\text{-}Ni}$ is the Ni extraction contents, %;
$C_{Ni\text{-}leached\ ore}$ is the content of the Ni in the ore after leaching, %;
$C_{Ni\text{-}fed}$ is the content of Ni in the ore fed to the reduction furnace, %;
$C_{Fe\text{-}fed}$ is the content of iron in the ore fed to the reduction furnace, %;
$C_{Fe\text{-}leached\ ore}$ is the content of iron in the ore after leaching, %.

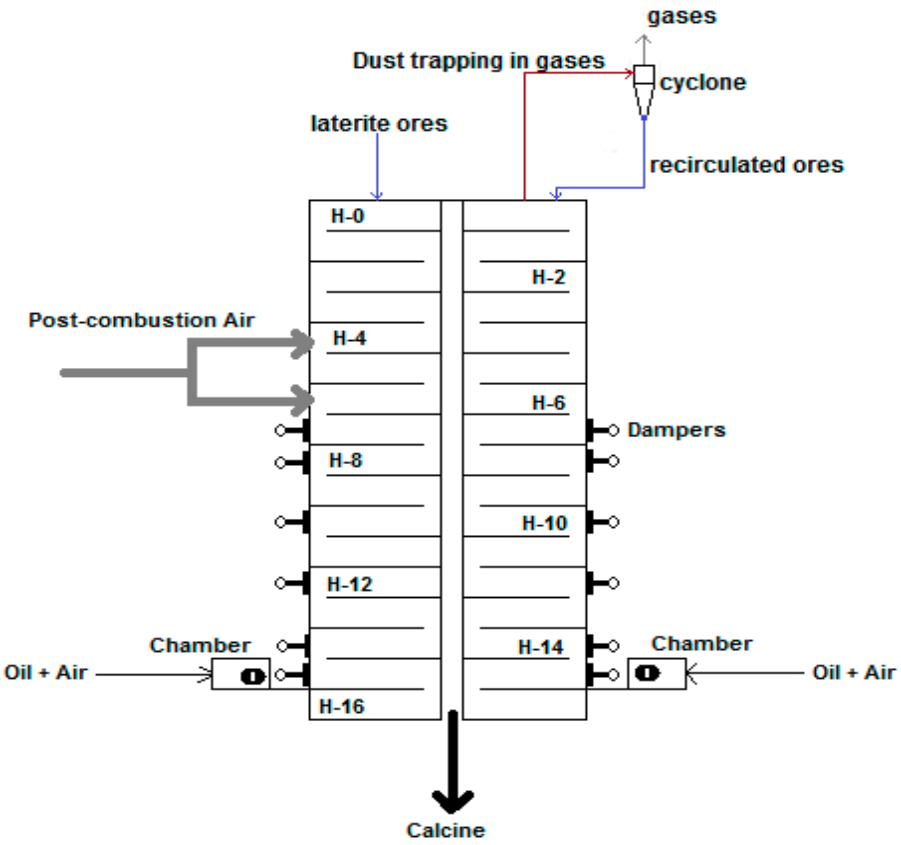

Figure 2. Pilot-plant-scale reduction furnace; letter H designates the hearth [9].

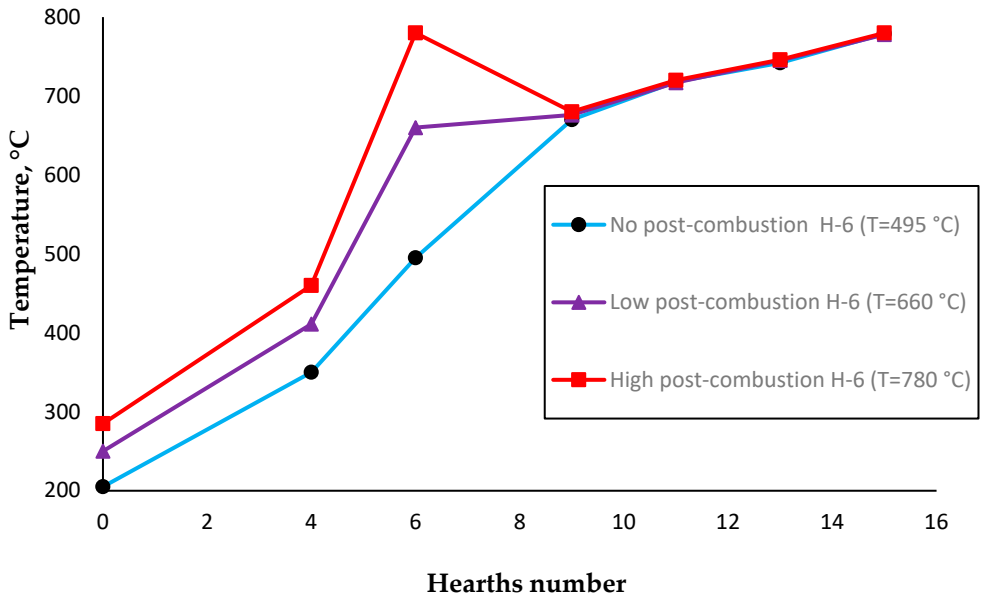

Figure 3. Temperature profiles in the reduction furnace.

2.3. Analytical Techniques

The chemical analyses of the samples were performed using atomic absorption spectrometry (AAS, model SOLAR 929, Solar System ATI, Unicam Analytical Technology Inc., Cambridge, UK), whilst the crystalline structure and composition of the fed lateritic ore were analyzed by powder X-ray diffraction (XRD) using a PANalytical X'PERT3 diffractometer (Malvern Panalytical, Doncaster, UK) with Gonio type sweep in [°2θ] angular registration from 4.0042 to 79.9962 with step distance in °2θ of 0.0080 with Cu radiation

and a nickel filter, potential difference of 40 kV, current of 30 mA, and a calibration checked by an external silicon standard scan.

Additionally, the morphology of the reduced lateritic ore was examined by Scanning Electron Microscopy using an X-ray Analyzer (Malvern Panalytical, Doncaster, UK). Images and spectra were obtained using a Tescan model 5130 SB microscope and an Oxford Instruments model Inca Energy 350 X-ray analyzer (Brno, Czech Republic). Particle size distribution analyses of the fed and reduced lateritic ore were determined using a Horiba LA 250V2 Particle Analyzer (Horiba Jobin Yvon Sas, Saint Albans, UK).

2.4. Methodology for Determining Kinetic Behavior

For each operating condition under analysis, the kinetic behavior was determined by following these steps:

(a) Verification of compliance and stability with the furnace operating conditions.
(b) Preparation of 9 samplers, previously coded with the number of each even-numbered furnace chamber, containing 200 mL of ammonia-carbonate liquor with an NH_3 concentration of 80–85 g/L.
(c) Determination of the mass of each sampler with the 200 mL of previously added liquor.
(d) Addition of an argon flow to each sampler to prevent the reoxidation process of the previously reduced samples taken from the even-numbered hearths.
(e) Collection of reduced ore samples from the even-numbered furnace hearts, from H-0 to H-16, with a 10 min interval between each sampler.
(f) Determination of the mass of reduced ore using the weight difference method.
(g) Leaching of the reduced mineral taken from each furnace hearth for 2 h with the ammonia-carbonate liquor with an NH_3 concentration of 80–85 g/L (liquid/solid ratio of 10:1) in stirred-tank reactors.
(h) Filtering and vacuum-washing the suspensions (formulated in g) with 200 mL of ammonia-carbonate solutions at (7 and 3%) and distilled water, respectively.
(i) Drying the filtered solid in the oven at 150 °C for 2 h.
(j) Cooling the dry solid to room temperature and grinding it until everything had a particle size of less than 0.150 mm.
(k) Homogenization of the ground solid and characterize the elements of interest in a certified analytical laboratory.
(l) Plotting the amount of residual Ni (%) of each of the leached solid samples as a function of time (min).

2.5. Methodology to Identify the Mechanism That Describes the Roasting/Reduction Process

In this investigation, the procedure proposed by Angulo et al. [32] was used to identify the mechanism describing the roasting/reduction process. The evaluated models are shown in Table 2.

Table 2. Mechanisms analyzed [x_{Ni} is the conversion ratio of Ni (degree of reduction) and t is the time, while k_{DGF}, k_{DAL}, k_{ChR}, k_{GN-2}, k_{GN-3}, and k_{GN-5} are the rate constants for each proposed mechanism].

Model Type	Mechanism	Equation
Unreacted core	Diffusion through the gas film (DGF)	$x_{Ni} = k_{DGF}t$
	Diffusion through the ash layer (DAL)	$1 - 3\left(1 - x_{Ni}\right)^{\frac{2}{3}} + 2(1 - x_{Ni}) = k_{DAL}t$
	Chemical reaction (ChR)	$1 - \left(1 - x_{Ni}\right)^{1/3} = k_{ChR}t$

Table 2. *Cont.*

Model Type	Mechanism	Equation
Nucleation	2-D growth of nuclei (GN-2)	$[-\ln(1-x_{Ni})]^{1/2} = k_{GN\text{-}2}t$
	3-D growth of nuclei (GN-3)	$[-\ln(1-x_{Ni})]^{1/3} = k_{GN\text{-}3}t$
	5-D growth of nuclei (GN-5)	$[-\ln(1-x_{Ni})]^{1/5} = k_{GN\text{-}5}t$

3. Results and Discussions

3.1. Chemical-Physical Characteristics of the Reduced Mineral

The main chemical and physical characteristics of the reduced ore are presented in Table 3. The results indicate that the selective reduction roasting process is adequate, since the transformation of NiO into metallic nickel (Ni^0) is enhanced, as the formation of metallic iron (Fe^0) is controlled with values below 3%. The high contents of Fe (46.53%) and magnetic fraction (59.63%) indicate that the reduced ore is dominated by magnetite as the main mineralogical phase—a result that can be corroborated in Figures 4 and 5.

Table 3. Chemical-physical characteristics of the reduced mineral [[a] average, [b] standard deviation, [c] apparent density, [d] magnetic fraction].

Statistics	Content, wt %									ρ [c], kg/m^3	MF [d], %
	Ni	Co	Fe	Ni^0	Fe^0	Fe^{2+}	FeO	S	C		
A [a]	1.34	0.112	46.53	1.07	2.78	25.06	19.90	0.60	1.37	4.560	59.63
σ [b]	0.04	0.00	0.27	0.58	0.06	0.23	0.24	0.06	0.05	9.42	1.86

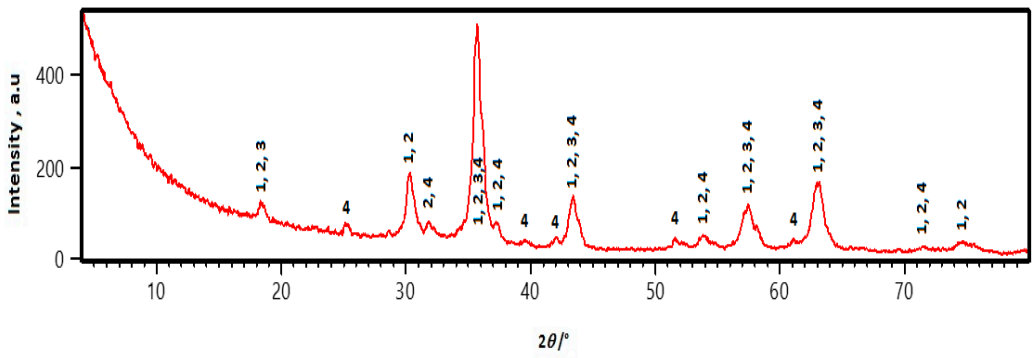

Figure 4. X-ray diffraction pattern of the reduced-leached mineral. 1—Magnetite, syn: Fe_3O_4; 2—Maghemite, syn: Fe_2O_3; 3—Magnesiochromite, ferroan: [(Mg, Fe)(Cr, Al)$_2O_4$]; 4—Fayalite: $Mg_{26}Fe_{1,74}(SiO_4)$.

The XRD results (Figure 4) and the distribution of elements in the reduced mineral (Figure 5) also allow us to identify the presence of the mineralogical phases Maghemite, Fayalite, and Ferroan Magnesiochromite; it was confirmed that the temperatures exceeding 700 °C in the lower hearths likely explain the persistence of unreduced Ni phases.

The identification of the Ni phases was not possible because its concentration is below the detection limit; see Figure 4. In general, the results described in this study coincide with reports made in different investigations [9,32–38].

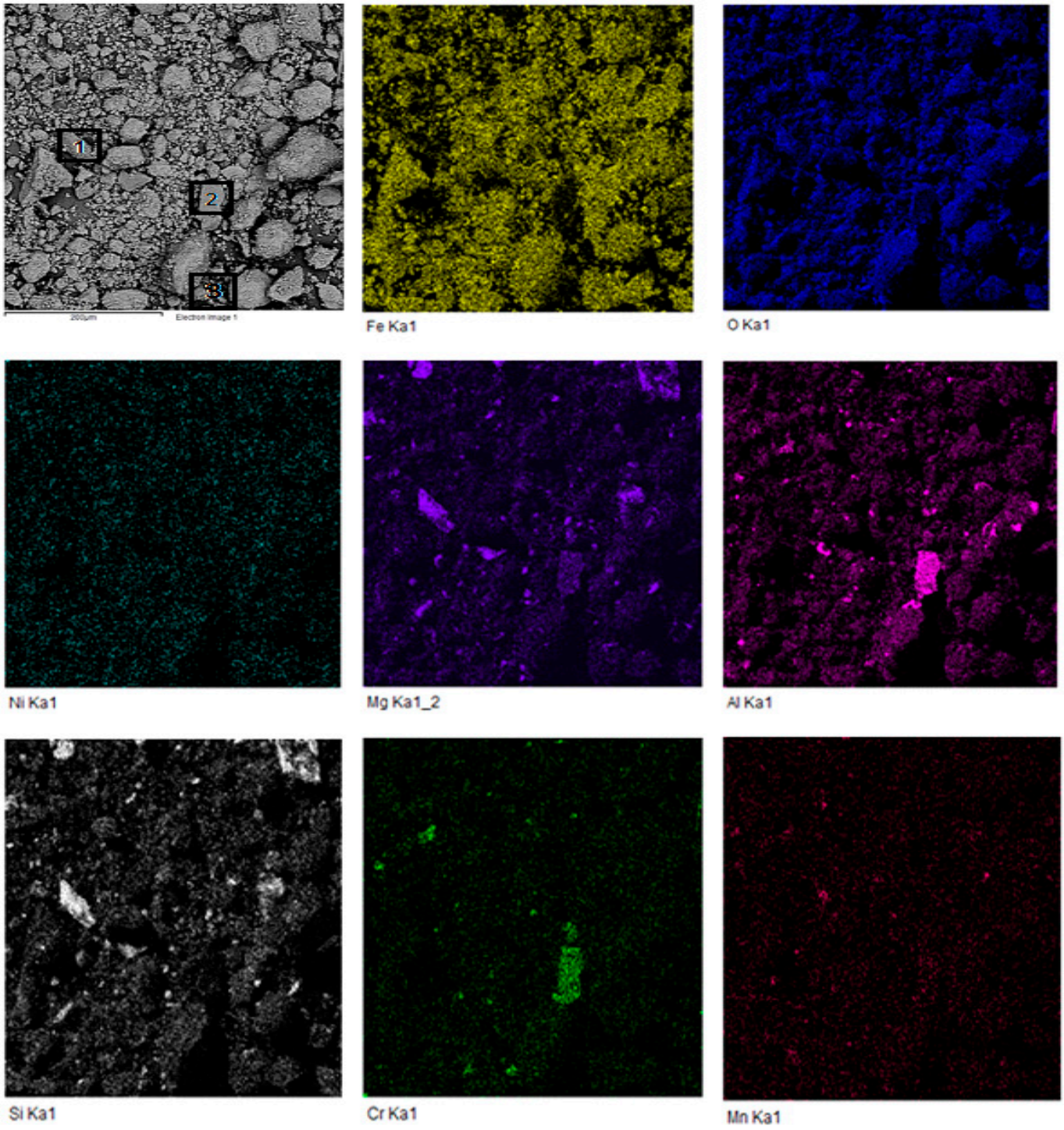

Figure 5. Photograph of the results of element mapping in the reduced mineral. The main mineralogical phases are as follows: 1—Fayalite: $Mg_{26}Fe_{1,74}(SiO_4)$ 2—Magnesiochromite, ferroan: [(Mg, Fe)(Cr, Al)$_2O_4$]; 3—Magnetite: Fe_3O_4.

Furthermore, it is important to highlight that the analysis of the chemical-physical characteristics shown in Table 3 and Figures 2 and 4 confirm that the Fe-phase transformation involves the following steps: Goethite (FeOOH) → Hematite (Fe_2O_3)→ Magnetite (Fe_3O_4) → Metal oxide (FeO) → Metallic iron (Fe), similar to those described in different studies [9,25,27,39].

3.2. Effect of Post-Combustion Air on the Reaction Rate Constant of the Roasting/Reduction Process

Figure 6 and Appendix A present the kinetic behavior of residual Ni % during the reduction process at different temperatures of the H-6 under study. The kinetics (k) of residual Ni% were characterized by a first-order reaction distribution with coefficients of determination greater than 0.9484, similar to that reported by Castellanos [40] during the evaluation of pyrite as a reducing additive. It is important to note that the significant changes shown by k as the post-combustion air-supply conditions varied are striking, as it regularly showed a behavior inversely proportional to the increase in temperature in H-6. This behavior can be justified by the dilution of the reducing gases generated by the air supply to the furnace in the heating zone. Furthermore, is observed that when the post-combustion air flow in H-6 decreases (see Figure 6 for the transformations starting at 20 min), the amount of residual Ni decreases considerably; this behavior can be explained by the early execution of the dehydroxylation processes of gohetite and lizardite, as suggested by various studies [28,41,42]. Regarding the shape of the curves, it suggests that the mechanism that best describes the roasting/reduction process is a combination of the diffusion model through the ash layer (DAL) and the growth of the nucleus (GN), being the controlling stage of the DAL, similar to that reported by Angulo et al. [32], regardless of the operating condition under analysis (see Appendix B).

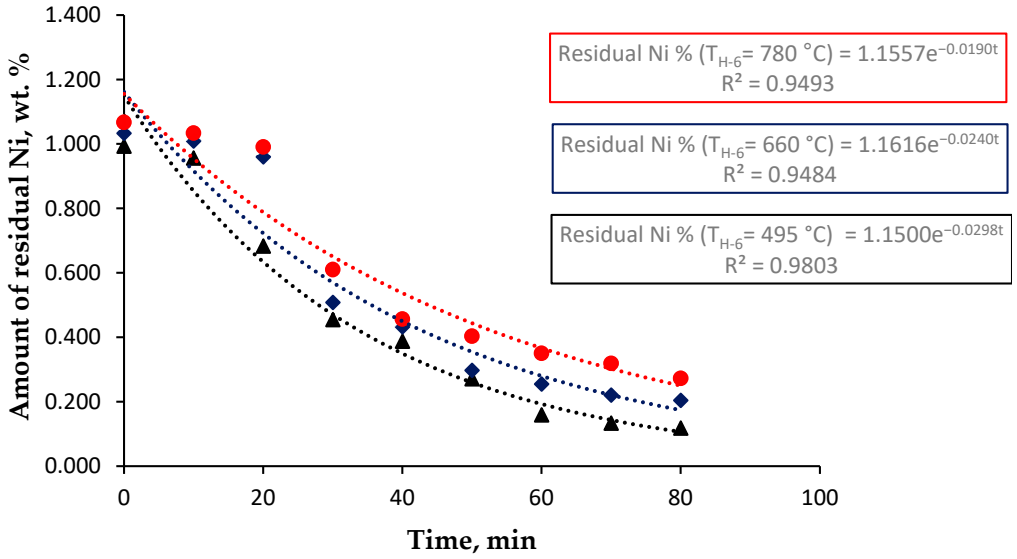

Figure 6. Kinetic behavior for different temperatures of H-6.

Figure 7 models the relationship between k and the increase in temperature of H-6 of the furnace. The model that best describes the relationship is a decreasing second-order polynomial with a coefficient of determination and residual error of 1.00 and 0.00, respectively, indicating that the increase in hearth temperature exerts a negative influence on the roasting/reduction process by decreasing k by 7.0938% for every 57 °C increase in the hearth temperature, with a confidence level of 95%.

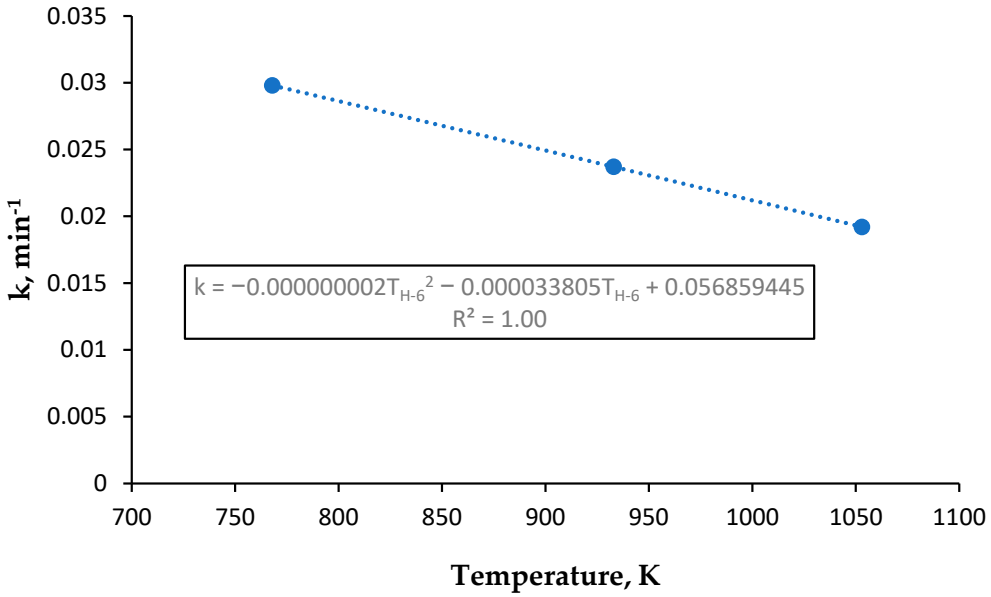

Figure 7. Reaction rate ratio (k) as a function of increasing temperature of H-6.

3.3. Effect of Post-Combustion Air on the Granulometric Behavior of the Reduced Ore

The effect of H-6 post-combustion air feed on the granulometry of the reduced mineral is shown in Figures 8 and 9. Regardless of the operating conditions used in the reactor, it is observed that the lateritic ore after the roasting/reduction process experiences a growth in the average diameter of its particles, where the main changes are shown in the particle sizes greater and less than 67 and 10 μm, respectively, with an increase in the maximum particle size of the reduced mineral (262,376 μm) of 23.77% compared to that of the lateritic ore (200 μm); see Figure 8.

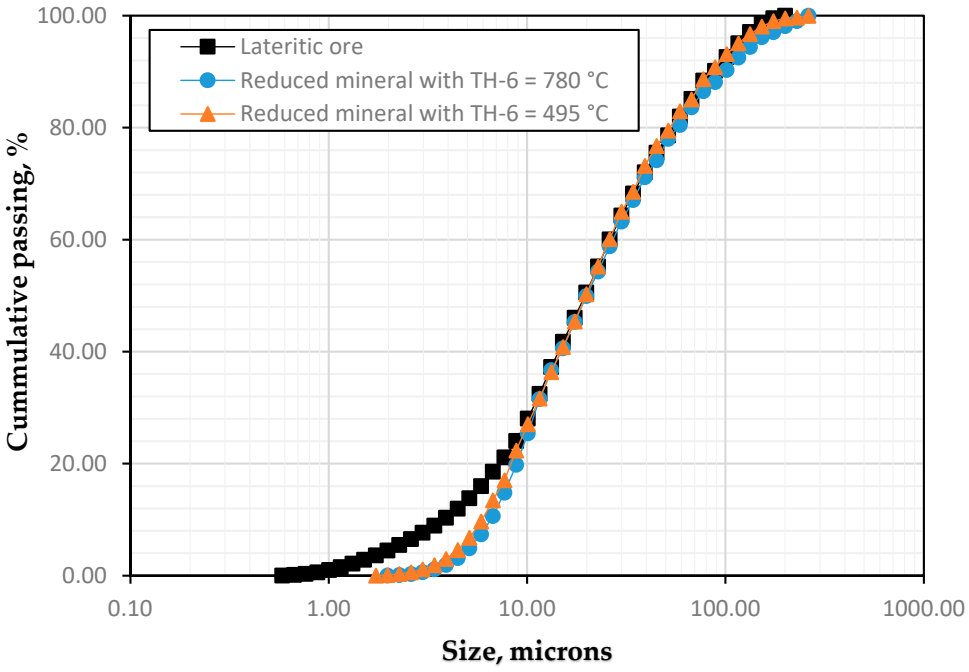

Figure 8. Granulometric behavior of ground lateritic ore and reduced mineral with and without post-combustion.

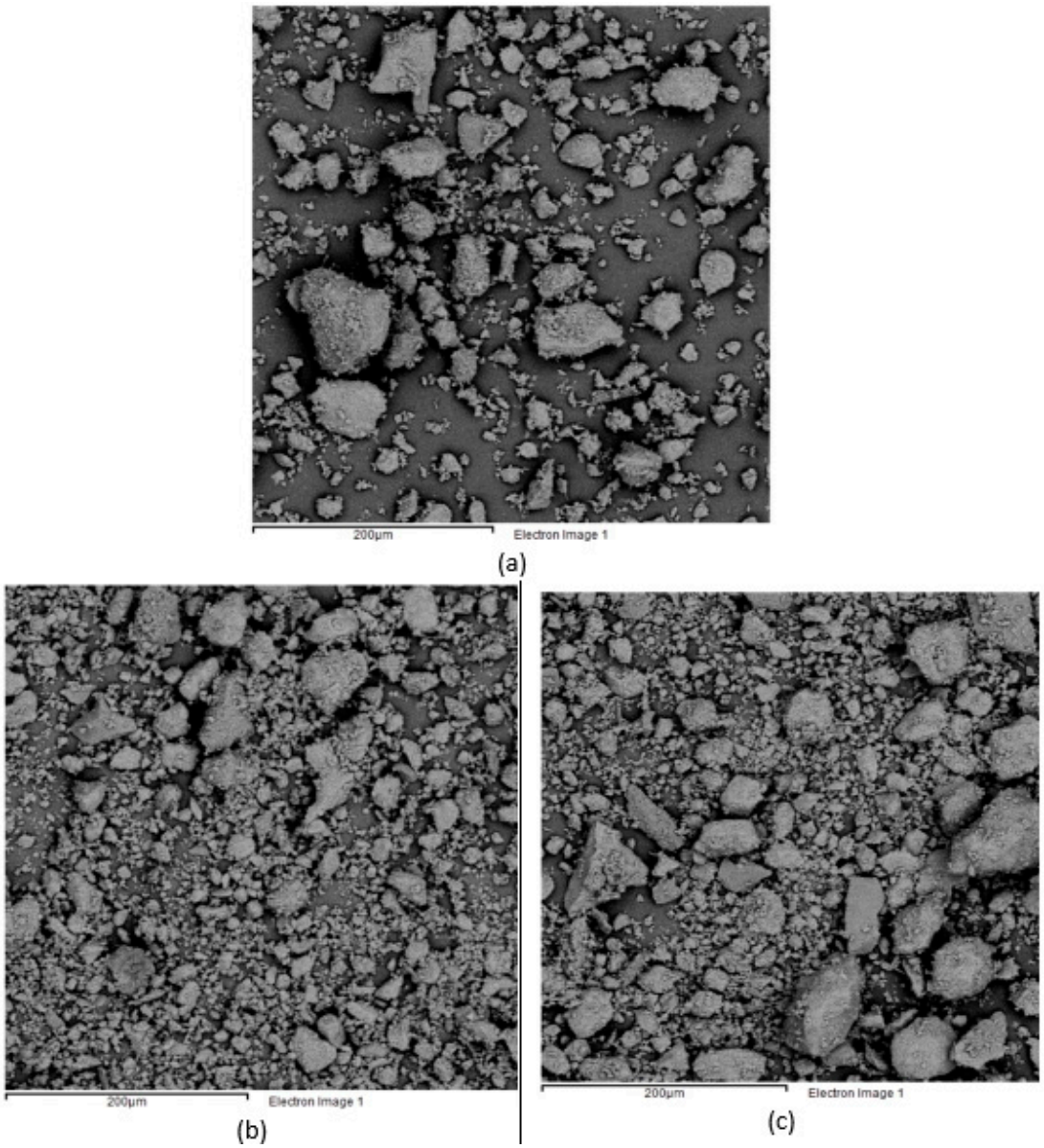

Figure 9. SEM of ground and reduced lateritic mineral. (**a**) Laterite ore fed into the hearth furnace. (**b**) Reduced mineral without post-combustion $T_{H\text{-}6}$ = 495 °C. (**c**) Reduced mineral with post-combustion $T_{H\text{-}6}$ = 780 °C.

The feeding of post-combustion air under the maximum operating conditions under study caused the average particle diameter to increase by 5.52 µm (17.49%) with a considerable degree of irregularity, while, in the case of the reduction process without post-combustion, the sizes are characterized by being more regular, with a small increase of 1.87 µm (6.68%); see Figures 8 and 9.

These results explain the mechanism behind the slowdown in the roasting/reduction process of lateritic ores during the introduction of post-combustion air into H-6, since, by causing a considerable increase in the sizes of the grains, the diffusive process of penetration and evacuation of the gases within the particle requires a longer residence time to guarantee a conversion similar to that achieved without the introduction of post-combustion air (see Appendix B).

3.4. Effect of Post-Combustion Air on Nickel Extraction

Figure 10 shows the behavior of the average Ni extractions as a function of H-6 temperature. It was observed that the extractions range from 82 to 91%, where the shape of the curve confirms the negative effect generated by the supply of post-combustion air on the extractions of the process, causing a decrease of 1.68% for every 57 °C increase in the hearth in a temperature range of 495–780 °C. Furthermore, the best-fitting mathematical model is a decreasing quadratic polynomial, with a coefficient of determination greater than 98% and an absolute error of 0.33%. It is important to note that these results coincide with those obtained at pilot scale when analyzing the effect of post-combustion in H-6 with the use of the reducing additive FO2.5 [10].

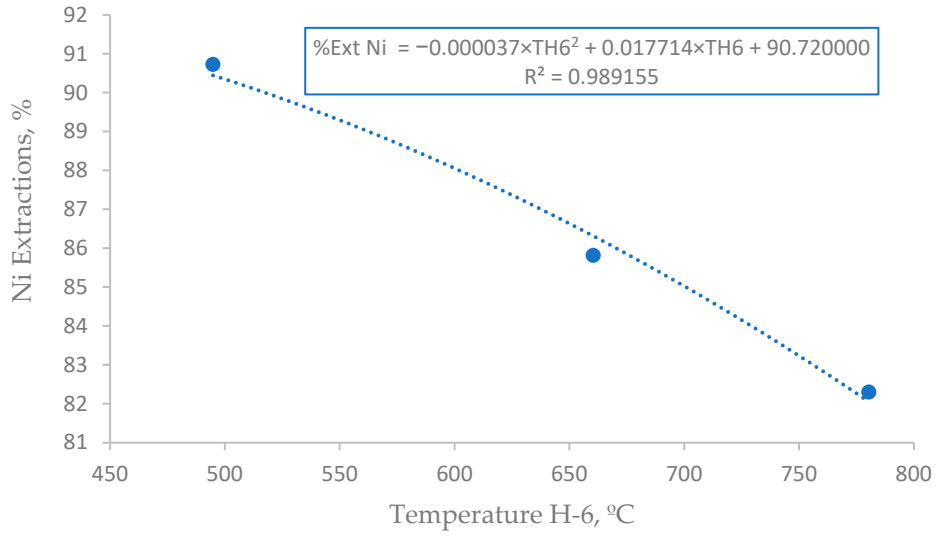

Figure 10. Ni extraction behavior with increasing H-6 temperature.

4. Conclusions

An evaluation of the effect of post-combustion air feeding was carried out in a conventional pilot-scale multi-hearth furnace by varying the temperature of H-6 from 495 °C (without post-combustion air) to 780 °C (the maximum post-combustion level evaluated). A comprehensive analysis of the results indicates that this variable causes a considerable decrease in Ni extraction in the roasting/reduction process. Specifically, when lateritic ores with a predominance of Fe oxides and oxyhydroxides are fed to the furnace, the following is shown:

- A decrease in the reaction rate of the roasting/reduction process (k decreases 7.0938% for every 57 °C of temperature increase in H-6).
- A considerable increase in the average particle size, making the diffusive processes controlling the process difficult.

These results suggest that, in the future, industrial plants will need to implement dust recovery systems that allow for the elimination of post-combustion air. In this sense, one technological option is to replace electrofilters with bag filters that contain elements capable of withstanding temperatures above 500 °C. On the other hand, if this variable is to continue to be used, it is recommended that H-6 temperatures operate within the range of 680–700 °C as an alternative to minimize the losses of the Ni extractions. Therefore, control of the post-combustion air feed is a high priority to ensure maximum Ni extraction levels in the Caron process.

Author Contributions: Conceptualization, H.J.A.P. and M.S.; Data curation, H.J.A.P.; Formal analysis, H.J.A.P., F.M.G.M., I.S. and I.J.; Investigation, H.J.A.P., N.T., J.C., I.J., E.S.-R. and M.S.; Methodology, H.J.A.P., J.C., F.M.G.M., I.S., I.J. and M.S.; Project administration, N.T. and M.S.; Resources, N.T.; Software, H.J.A.P.; Supervision, N.T. and M.S.; Validation, H.J.A.P., J.C., F.M.G.M., I.S. and E.S.-R.; Visualization, H.J.A.P.; Writing—original draft, H.J.A.P.; Writing—review and editing, H.J.A.P., N.T., E.S.-R. and M.S. All authors have read and agreed to the published version of the manuscript.

Funding: This research received no funding.

Data Availability Statement: The original contributions presented in this study are included in the article. Further inquiries can be directed to the corresponding author.

Acknowledgments: M.S. acknowledges the infrastructure and support from "Doctorado en Ingeniería de Procesos de Minerales" at the Universidad de Antofagasta. The authors would like to thank the Programa de Doctorado en Energía Solar of the Universidad de Antofagasta, Chile; the support of ANID-Chile through the research project FONDECYT Iniciación 11230550; the Project DIUDA N° 22430 carried out by the Facultad de Ingeniería of the Universidad de Atacama; and ANID/FONDAP 1523A0006 Solar Energy Research Center SERC-Chile, 2nd extension. The authors have reviewed and edited the output, and take full responsibility for the content of this publication.

Conflicts of Interest: The authors declare no conflicts of interest.

Appendix A

Table A1. Amount of residual Ni in the different zones of the furnace without post-combustion air supply (TH-6 = 495 °C).

Time, min	1	2	3	Average
0	0.980	1.010	0.990	0.993
10	0.950	0.980	0.940	0.957
20	0.695	0.750	0.605	0.683
30	0.435	0.410	0.520	0.455
40	0.376	0.367	0.421	0.388
50	0.251	0.285	0.277	0.271
60	0.147	0.171	0.159	0.159
70	0.130	0.139	0.131	0.133
80	0.112	0.123	0.119	0.118

Table A2. Amount of residual Ni in the different zones of the furnace with post-combustion air supply (T_{H-6} = 660 °C).

Time, min	1	2	3	Average
0	1.050	1.020	1.030	1.033
10	0.997	1.010	1.020	1.009
20	0.970	0.960	0.950	0.960
30	0.533	0.503	0.489	0.508
40	0.408	0.466	0.424	0.433
50	0.271	0.306	0.315	0.297
60	0.255	0.277	0.232	0.255
70	0.213	0.229	0.219	0.220
80	0.198	0.210	0.205	0.204

Table A3. Amount of residual Ni in the different zones of the furnace with post-combustion air supply (T_{H-6} = 780 °C).

Time, min	1	2	3	Average
0	1.056	1.067	1.078	1.067
10	1.022	1.030	1.050	1.034
20	0.983	0.980	1.010	0.991
30	0.581	0.616	0.633	0.610
40	0.430	0.460	0.479	0.456
50	0.409	0.380	0.420	0.403
60	0.320	0.350	0.380	0.350
70	0.300	0.310	0.347	0.319
80	0.281	0.259	0.276	0.272

Appendix B

Table A4. Complete Reaction Time for the evaluated mechanisms.

Temperature H-6, °C	Complete Reaction Time, min					
	Chemical Reaction (ChR)	Diffusion		Growth of Nuclei		
		Through the Gas Film (DGF)	Through the Ash Layer (DAL)	GN-2	GN-3	GN-5
495	146	77	161	48	51	54
660	174	85	211	53	55	56
780	203	94	277	59	59	59

Table A5. Complete Reaction Time for the evaluated mechanisms. Evaluation of experimental and estimated times in the best combination of mechanisms (DAL and GN-3) that describe the roasting/reduction process.

Experimental Time, min	Estimated Time, min		
	T_{H-6} (780 °C)	T_{H-6} (660 °C)	T_{H-6} (495 °C)
0	0	0	0
10	9	8	8
20	12	12	21
30	35	36	34
40	49	43	39
50	55	58	50
60	62	64	66
70	67	69	71
80	74	72	74
R^2	**0.9623**	**0.9576**	**0.9835**
Residual Error	**5.32**	**5.72**	**3.46**

References

1. Topak, A.; Toprak Döşlü, S. Electrochemical Tuning of Ni-Fe Catalysts Using Various Techniques for Efficient Hydrogen Evolution in Alkaline Media. *Processes* **2025**, *13*, 644. [CrossRef]
2. Sang, P.; Luo, W.; Li, W.; Wang, C.; Chen, Y.; Zhou, L.; Ma, Z.; Wang, D.; Duan, Y. A Novel Martensitic Stainless Steel Material for CO_2 Corrosion Environment. *Processes* **2024**, *12*, 2912. [CrossRef]

3. Valencia, F.; Rabbani, M.; Fahimi, A.; Vahidi, E. Assessing the environmental burden of nickel sulfate for batteries: A life cycle perspective. *Res. Conserv. Recycl.* **2025**, *215*, 108130. [CrossRef]
4. Lv, W.; Makuza, B.; Wang, F.; Marcuson, S.; Barati, M. A Review of Direct Reduction–Magnetic Separation Process for Ferronickel Production from Nickel Laterite. *J. Sustain. Metall.* **2025**, *11*, 3–28. [CrossRef]
5. Wang, M.; Fan, Q.; Bai, Z.; Yuan, S.; Li, Y.; Han, Y. Semi-industrial experiment on efficient preparation of nickel-iron alloy from laterite nickel ore: A suspension roasting pre-reduction electric furnace melting (SRPEF) process. *J. Taiwan Inst. Chem. Eng.* **2025**, *173*, 106164. [CrossRef]
6. Zevgolis, E.N.; Daskalakis, K.A. Nickel Prod. The Nickel Production Methods from Laterites and the Greek Ferronickel Production among Them. *Mater. Proc.* **2022**, *5*, 104. [CrossRef]
7. Chen, J.; Zhong, Y.; Wang, B.; Luo, J.; Peng, Z.; Chen, Y.; Li, G.; Rao, M. Sodium sulfate-assisted reductive roasting for enhanced Ni and Co recovery from limonitic laterite: Mechanism and pilot-scale rotary-kiln validation. *Int. J. Miner. Metall. Mater.* **2025**. [CrossRef]
8. Caron, M.H. Process of Recovering Values from Nickel and Cobalt-Nickel Ores. U.S. Patent 1 487 145, 18 March 1924.
9. Angulo Palma, H.J.; Legrá, Á.L.; Urgellés, A.L.; Pedrera, C.H.; Gallegos, S.; Galleguillos, M.F.M.; Toro, N. Use of a mixture of coal and oil as an additive for selective reduction of lateritic ore by the Caron process. *Hem. Ind.* **2024**, *78*, 17–27. [CrossRef]
10. Angulo Palma, H.J.; Legrá Legrá, A.; Lamorú Urgellés, A.; Gálvez, E.; Castillo, J. Post-combustion Effect on Nickel and Cobalt Extractions from the Caron Process. In Proceedings of the Fourth International Conference on Inventive Material Science Applications. Advances in Sustainability Science and Technology; Bindhu, V., Tavares, J.M.R.S., Ţălu, Ş., Eds.; Springer: Singapore, 2022; pp. 515–527. [CrossRef]
11. Rojas Vargas, A.; Magaña Haynes, M.E.; Riverón, A.R. Lixiviación carbonato amoniacal: Estimación del níquel disuelto en el efluente de destilación. *Rev. De Metal.* **2019**, *55*, e149. [CrossRef]
12. Canterford, J. Oxide Ores of Nickel—The Australian Situation. *Miner. Procesing Extr. Metall. Rev.* **1983**, *1*, 85–109. [CrossRef]
13. Caron, M.H. Fundamental and practical factors in ammonia leaching of nickel and cobalt ores. *JOM-J. Miner. Met. Mater. Soc.* **1950**, *2*, 67–90. [CrossRef]
14. De Graaf, J. The treatment of lateritic nickel ores—A further study of the Caron process and other possible improvements. *Part I. Effect of reduction conditions. Hydrometallurgy* **1979**, *5*, 47–65. [CrossRef]
15. Chander, S.; Sharma, V. Reduction roasting/ammonia leaching of nickeliferous laterites. *Hydrometallurgy* **1981**, *7*, 315–327. [CrossRef]
16. Chen, J.-h.; Jak, E.; Hayes, P. Investigation of the reduction roasting of saprolite ores in the Caron process: Microstructure evolution and phase transformations. *Miner. Process. Extr. Metall.* **2019**, *130*, 148–159. [CrossRef]
17. Chen, J.; Jak, E.; Hayes, P. Investigation of the reduction roasting of saprolite ores in the Caron process: Reaction mechanisms and reduction kinetics. *Miner. Process. Extr. Metall.* **2019**, *130*, 425–432. [CrossRef]
18. Angulo Palma, H.J. Sustitución Del Petróleo Aditivo Por Carbón Bituminoso En El Proceso De Tostación/Reducción De La Tecnología Caron. Ph.D. Thesis, Universidad de Oriente, Santiago de Compostela, Cuba, 11 April 2024.
19. Mano, E.S.; Caner, L.; Petit, S.; Chaves, A.P.; Mexias, A.S. Ni-smectitic ore behaviour during the Caron process. *Hydrometallurgy* **2019**, *186*, 200–209. [CrossRef]
20. Coello Velázquez, A.L.; Llorente Arce, L.; García, A. Efecto del petróleo aditivo en los indicadores energo-tecnológicos en los circuitos cerrados de molienda del mineral laterítico a nivel industrial. *Min. Y Geol.* **2020**, *36*, 316–327.
21. Véliz Jardines, A.I.; Miranda López, J. Desarrollo de investigaciones sobre la tecnología Caron durante el procesamiento de las lateritas de baja ley de níquel y de los escombros lateríticos, clasificados como: Menas o minerales no industriales. *Tecnol. Química* **2022**, *42*, 361–383.
22. Kawahara, M.; Toguri, J.; Bergman, R. Reducibility of laterite ores. *Metall. Trans. B* **1988**, *19*, 181–186. [CrossRef]
23. Ramírez Pérez, I.M.; Ramírez Serrano, B. Efecto de la postcombustión sobre los principales índices técnico-económicos en un horno Herreshoff para la producción de níquel. *Min. Y Geol.* **2021**, *37*, 426–444.
24. Rojas Vargas, A.; Sánchez Guillen, C.; Magaña Haynes, M.E.; Hernández Pedrera, C. Extracción potencial de níquel y cobalto con mineral laterítico de mina "Pinares de Mayarí" en la tecnología Caron. *Parte II. Tecnol. Química* **2022**, *42*, 405–419.
25. Ilyas, S.; Kim, H.; Srivastava, R.R. Carbothermic Reduction Roasting of a Low-Grade Nickel Laterite Ore in the Modified Caron Process. In *Ni-Co 2021: The 5th International Symposium on Nickel and Cobalt*; Anderson, C., Goodall, G., Gostu, S., Gregurek, D., Lundström, M., Meskers, C., Nicol, S., Peuraniemi, E., Tesfaye, F., Tripathy, P.K., et al., Eds.; The Minerals, Metals & Materials Series; Springer: Berlin/Heidelberg, Germany, 2021; pp. 317–328. [CrossRef]
26. Ilyas, S.; Srivastava, R.R.; Kim, H.; Ilyas, N.; Sattar, R. Extraction of nickel and cobalt from a laterite ore using the carbothermic reduction roasting-ammoniacal leaching process. *Sep. Purif. Technol.* **2020**, *232*, 115971. [CrossRef]
27. De Alvarenga Oliveira, V.; Dos Santos, C.G.; De Albuquerque Brocchi, E. Assessing the influence of NaCl on the reduction of a siliceous laterite nickel ore under Caron process conditions. *Metall. Mater. Trans. B* **2019**, *50*, 1309–1321. [CrossRef]

28. Valix, M.; Cheung, W. Effect of sulfur on the mineral phases of laterite ores at high temperature reduction. *Miner. Eng.* **2002**, *15*, 523–530. [CrossRef]
29. Ramírez Mendoza, M. Modelación del proceso de postcombustión en un horno de reducción de níquel. *Rev. De Metal.* **2002**, *38*, 150–157. [CrossRef]
30. Santana Lopez, E.; Montero Góngora, D.; Vega Arias, O.V. Identification of the Air Supply System for Combustion, with the Help of Artificial Neural Networks. *Biomed. J.* **2018**, *10*, 7714–7717. [CrossRef]
31. Montero Góngora, D.; Columbié Navarro, Á.; Montero Laurencio, R.; Trujillo Codorniú, R.; Vázquez Seisdedos, L. Modelo NARX de la postcombustión en un horno de reducción de mineral laterítico. *Rev. Ing. Electrónica Automática Y Comun.* **2022**, *43*, 1–14.
32. Angulo Palma, H.J.; Saldana, M.; Legrá, Á.L.; Urgellés, A.L.; Pedrera, C.H.; Gallegos, S.; Galleguillos, M.F.M.; Toro, N. Kinetic behaviour of the roasting/selective reduction process with the use of a mixture of bituminous coal and fuel oil as the additive. *Hem. Ind.* **2025**, *79*, 69–77. [CrossRef]
33. Rhamdhani, M.; Hayes, P.; Jak, E. Nickel laterite Part 1–microstructure and phase characterisations during reduction roasting and leaching. *Miner. Process. Extr. Metall.* **2009**, *118*, 129–145. [CrossRef]
34. Rhamdhani, M.; Chen, J.; Hidayat, T.; Jak, E.; Hayes, P. Advances in research on nickel production through the Caron process. In Proceedings of the European Metallurgical Conference 2009, Innsbruck, Austria, 28 June–1 July 2009; Harre, J., Ed.; GDMB: Clausthal-Zellerfeld, Germany, 2009; pp. 899–914, ISBN 978-3-940276-19-3.
35. Cabrera, G.; Gómez, J.M.; Hernández, I.; Coto, O.; Cantero, D. Different strategies for recovering metals from Caron process residue. *J. Hazard. Mater.* **2011**, *189*, 836–842. [CrossRef]
36. Rojas Vargas, A.; Magaaña Haynes, M.E.; del Toro Alvarez, D.; Angulo Palma, H.J.; Yasir AlJaberi, F.; Dawood Salman, A.; Mohsen Alardhi, S.; Mohammed, M.M.; Gabor' Gyurika, I.; Ihsan Ali, O. Nickel Mining: Studying the Kinetics and Modeling of Extraction Process from Laterite Ore. *South Afr. J. Chem. Eng.* **2025**, *53*, 362–372. [CrossRef]
37. Dung, N.Q.; Thuyet, N.M.; Oanh, N.T.H.; Viet, N.H. Fayalite formation under different heating techniques in iron ore composite briquette reduction. *Can. Metall. Q.* **2025**, 1–9. [CrossRef]
38. Zhang, X.; Wang, H.; Zhao, Y.; Luo, L.; Shen, L. Growth Behavior of Iron Grains During Reduction Roasting of Fayalite. *J. Sustain. Met.* **2024**, *10*, 2521–2533. [CrossRef]
39. Shofi, A.; Iman Supriyatna, Y.; Budi Prasetyo, A. Selective Reduction of Southeast Sulawesi Nickel Laterite using Palm Kernel Shell Charcoal: Kinetic Studies with Addition of Na_2SO_4 and NaCl as Additives. *Bull. Chem. React. Eng. Catal.* **2020**, *15*, 501–513. [CrossRef]
40. Castellanos Suárez, J. Cinética de la reducción de los minerales oxidados de níquel en Cuba. *Min. Y Geol.* **1984**, *2*, 197–222.
41. Valix, M.; Cheung, W. Study of phase transformation of laterite ores at high temperature. *Miner. Eng.* **2002**, *15*, 607–612. [CrossRef]
42. Marzoughi, O.; Anthony, W.; Rodrigues, F.; Elliott, R.; Peacey, J.; Pickles, C. Mechanism of carbothermic reduction of a sulfur-containing nickeliferous limonitic laterite ore. *Miner. Process. Extr. Metall.* **2020**, *129*, 267–281. [CrossRef]

Disclaimer/Publisher's Note: The statements, opinions and data contained in all publications are solely those of the individual author(s) and contributor(s) and not of MDPI and/or the editor(s). MDPI and/or the editor(s) disclaim responsibility for any injury to people or property resulting from any ideas, methods, instructions or products referred to in the content.